

Dynamics of Electron Currents in Nanojunctions with Time-Varying Components and Interactions

Eduardo C. Cuansing^{1,a)}, Francis A. Bayocboc² and Christian M. Laurio³

¹*Institute of Mathematical Sciences and Physics, University of the Philippines, Los Baños, Laguna 4031, Philippines*

²*School of Mathematics and Physics, University of Queensland, Queensland 4072, Australia*

³*Nara Institute of Science and Technology, 8916-5 Takayama, Ikoma, Nara 630-0192, Japan*

^{a)}Corresponding author: eccuansing@up.edu.ph

Abstract. We study the dynamics of the electron current in nanodevices where there are time-varying components and interactions. These devices are a nanojunction attached to heat baths and with dynamical electron-phonon interactions and a nanojunction with photon beams incident and reflected at the channel. We use the two-time nonequilibrium Green's functions technique to calculate the time-dependent electron current flowing across the devices. We find that whenever a sudden change occurs in the device, the current takes time to react to the abrupt change, overshoots, oscillates, and eventually settles down to a steady value. With dynamical electron-phonon interactions, the interaction gives rise to a net resistance that reduces the flow of current across the device when a source-drain bias potential is attached. In the presence of dynamical electron-photon interactions, the photons drive the electrons to flow. The direction of flow, however, depends on the frequencies of the incident photons. Furthermore, the direction of electron flow in one lead is exactly opposite to the direction of flow in the other lead thereby resulting in no net change in current flowing across the device.

MODELING THE NANODEVICES

The advent of nanometer-scale electronics has led to compact smart devices containing considerable computing power. As the sizes of electronic components shrink, however, electrons in the devices are restricted to flow within very confined dimensions. In such cases, quantum-mechanical and nonequilibrium effects are important. In this paper, we study the dynamics of electron currents in nanojunctions with time-varying components and interactions. We use the two-time nonequilibrium Green's function technique to calculate the current flowing across the devices.[1, 2] The nonequilibrium Green's function technique can be used in the study of many-body quantum systems that are partitioned into sub-parts. For example, the technique has been used in the study of transport through quantum dots,[3, 4, 5] a nanorelay,[6] a carbon nanotube transistor,[7] photon-assisted tunneling devices,[8] and a nanojunction with a time-varying gate potential.[9] In this paper, we study electron transport in a nanojunction attached to heat baths with dynamical electron-phonon interactions and a nanojunction with an incident photon beam striking the channel.

Shown in Fig. 1(a) is an illustration of a nanojunction with left and right heat baths attached to the channel. The heat baths have temperatures $T_{HB}^L > T_{HB}^R$ and therefore phonons flow from the left to the right heat bath. The direction of electron flow, on the other hand, depends on the sign of the source-drain bias potential V_b . We call the source as the left lead and the drain as the right lead. The left and right leads have chemical potentials μ_L and μ_R and temperatures T_e^L and T_e^R . We use the tight-binding approximation to model the devices. The Hamiltonian for the left and right leads are $H_e^L = \sum \varepsilon_k^L a_k^\dagger a_k + \sum v_{kj}^L (a_k^\dagger a_j + a_j^\dagger a_k)$ and $H_e^R = \sum \varepsilon_k^R b_k^\dagger b_k + \sum v_{kj}^R (b_k^\dagger b_j + b_j^\dagger b_k)$, where a_k and a_k^\dagger are the electron annihilation and creation operators at site k in the left lead, b_k and b_k^\dagger are the annihilation and creation operators at site k in the right lead, the ε_k^L and ε_k^R are the on-site energies at site k , the v_{kj}^L and v_{kj}^R are the hopping parameters for nearest-neighbor sites k and j , and the sums are over all sites in the leads. The leads are connected to the channel with the leads-channel coupling Hamiltonian $H_e^{LC} = v_{01}^{LC} (a_0^\dagger c_1 + c_1^\dagger a_0)$ and $H_e^{RC} = v_{21}^{RC} (c_1^\dagger b_2 + b_2^\dagger c_1)$, where $v_{01}^{LC} = v_{10}^{CL}$ and $v_{21}^{RC} = v_{12}^{CR}$ are the symmetric leads-channel coupling parameters. The Hamiltonian for the phonons in the left and right heat baths are $H_p^L = \sum \hbar k_k^L q_k^\dagger q_k + \sum \hbar \kappa_{jk}^L q_j^\dagger q_k$ and $H_p^R = \sum \hbar k_k^R r_k^\dagger r_k + \sum \hbar \kappa_{jk}^R r_j^\dagger r_k$, where $\hbar k_k^L$ and $\hbar k_k^R$ are the on-site

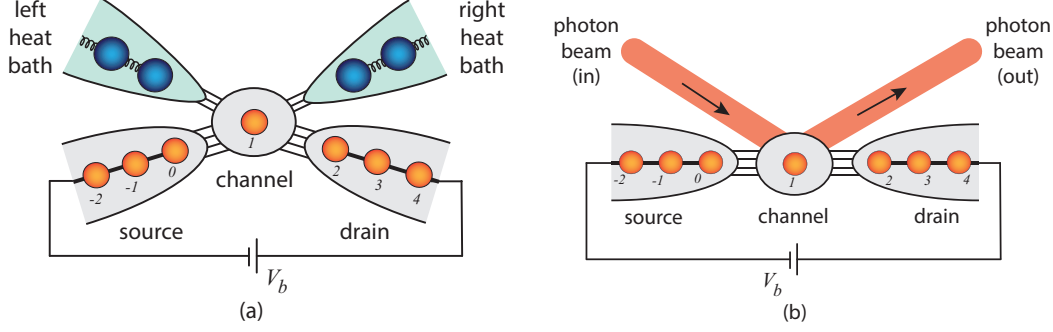


FIGURE 1. An illustration of the nanojunctions with (a) attached heat baths and (b) an incident photon beam. Electrons flow from the source, through the channel, and then on to the drain. The source-drain bias potential is V_b . In (a), electrons and phonons interact within the channel. In (b), the incident photons interact with the electrons flowing within the channel.

energies of the phonons at site k in the heat baths, $\hbar\kappa_{jk}^L$ and $\hbar\kappa_{jk}^R$ are the phonon hopping parameters between nearest-neighbor sites j and k , q_k^\dagger and q_k are the phonon creation and annihilation operators at site k in the left heat bath, and r_k^\dagger and r_k are the phonon creation and annihilation operators at site k in the right heat bath. The heat baths are coupled to the channel via $H_p^{LC} = \hbar\kappa_{01}^{LC} (q_0^\dagger p_1 + p_1^\dagger q_0)$ and $H_p^{RC} = \hbar\kappa_{21}^{RC} (r_2^\dagger p_1 + p_1^\dagger r_2)$, where p_1^\dagger and p_1 are the phonon creation and annihilation operators in the channel. The Hamiltonian in the channel contains an electron part $H_e^C = \varepsilon_1^C c_1^\dagger c_1$, a phonon part $H_p^C = \hbar\kappa_1^C p_1^\dagger p_1$, and the time-dependent electron-phonon interaction term $H_{ep}^C(t) = M_{ep}(t) (p_1^\dagger + p_1) c_1^\dagger c_1$, where $M_{ep}(t)$ is the electron-phonon interaction coupling parameter.[10, 11, 12] The total Hamiltonian of the device is $H = H_e + H_p + H_{ep}(t)$, where the time-independent electron part is $H_e = H_e^L + H_e^R + H_e^C + H_e^{LC} + H_e^{RC}$, the time-independent phonon part is $H_p = H_p^L + H_p^R + H_p^C + H_p^{LC} + H_p^{RC}$, and the time-dependent electron-phonon interaction term is in $H_{ep}(t) = H_{ep}^C(t)$.

We also study a nanojunction where a photon beam is incident on the channel, as illustrated in Fig. 1(b). The time-independent electron part of the Hamiltonian, H_e , is the same as in the previous device. The time-independent photon part of the Hamiltonian includes $H_\gamma = H_\gamma^L + H_\gamma^R + H_\gamma^C + H_\gamma^{LC} + H_\gamma^{RC}$. The Hamiltonian in the incident and reflected photon beams are $H_\gamma^L = \sum \chi_k^L \alpha_k^\dagger \alpha_k + \sum u_{jk}^L \alpha_j^\dagger \alpha_k$ and $H_\gamma^R = \sum \chi_k^R \beta_k^\dagger \beta_k + \sum u_{jk}^R \beta_j^\dagger \beta_k$, where χ_k^L and χ_k^R are the photon on-site energy at site k in the beams, u_{jk}^L and u_{jk}^R are the photon hopping parameters for nearest neighbors j and k , α_k^\dagger and α_k are the photon creation and annihilation operators in the left incident beam, β_k^\dagger and β_k are the photon creation and annihilation operators in the right reflected beam, and the sums are over all sites in the photon beams. The beam-channel coupling parts of the Hamiltonian are $H_\gamma^{LC} = u_{01}^{LC} (\alpha_0^\dagger \gamma_1 + \gamma_1^\dagger \alpha_0)$ and $H_\gamma^{RC} = u_{21}^{RC} (\beta_2^\dagger \gamma_1 + \gamma_1^\dagger \beta_2)$, where γ_1^\dagger and γ_1 are the photon creation and annihilation operators at the site in the channel. The channel part of the Hamiltonian contains the time-independent electron part $H_e^C = \varepsilon_1^C c_1^\dagger c_1$, the time-independent photon part $H_\gamma^C = \chi_1^C \gamma_1^\dagger \gamma_1$, and the part containing the time-dependent electron-photon interaction $H_{e\gamma}^C(t) = M_{e\gamma}(t) (\gamma_1 e^{-i\omega t} + \gamma_1^\dagger e^{i\omega t}) c_1^\dagger c_1$, where $M_{e\gamma}(t)$ is the electron-photon interaction strength and ω is the frequency of the photon.[8, 11, 13] The total Hamiltonian for the device is $H = H_e + H_\gamma + H_{e\gamma}(t)$ where H_e is the time-independent electron part, H_γ is the time-independent photon part, and $H_{e\gamma}(t) = H_{e\gamma}^C(t)$ is the time-dependent electron-photon interaction term in the channel.

The electron current flowing out of the left lead can be determined from the time rate of change of the number of electrons in the lead. Let $N^L = \sum a_k^\dagger a_k$ be the number operator in the left lead. Then, the current out of the left lead is

$$I^L(t) = \left\langle -q \frac{dN^L}{dt} \right\rangle = -\frac{iq}{\hbar} \langle [H, N^L] \rangle = -\frac{iq}{\hbar} v_{01}^{LC} (-\langle a_0^\dagger c_1 \rangle + \langle c_1^\dagger a_0 \rangle) = 2q \text{Re} \left[v_{01}^{LC} G_{10}^{CL,<}(t, t) \right], \quad (1)$$

where the Heisenberg equation of motion is used in the second equality, the $\text{Re}[\]$ indicates the real part, and the lesser nonequilibrium Green's function is $G_{10}^{CL,<}(t_1, t_2) = \frac{i}{\hbar} \langle a_0^\dagger(t_2) c_1(t_1) \rangle$. Similarly, the electron current flowing out of the right lead is

$$I^R(t) = \left\langle q \frac{dN^R}{dt} \right\rangle = -2q \text{Re} \left[v_{21}^{RC} G_{12}^{CR,<}(t, t) \right], \quad (2)$$

where the lesser nonequilibrium Green's function $G_{12}^{\text{CR},<}(t_1, t_2) = \frac{i}{\hbar} \langle b_2^\dagger(t_2) c_1(t_1) \rangle$. The results are the same for the two Hamiltonians we defined for the two types of nanojunctions we are studying. Note that in both Eqs. (1) and (2) a positive current means it is flowing into the right lead while a negative current means it is flowing into the left lead.

The lesser nonequilibrium Green's functions needed to determine the left and right currents can be calculated following the Keldysh-Schwinger formalism where time is on a Keldysh contour in a complex contour-time plane.[1, 2] We start with the contour-ordered Green's function $G_{10}^{\text{CL}}(\tau_1, \tau_2) = -\frac{i}{\hbar} \langle T_c c_1(\tau_1) a_0^\dagger(\tau_2) \rangle$, where τ_1 and τ_2 are contour-time variables and T_c is the contour-ordering operator. In the Interaction Picture, the contour-ordered Green's function becomes $G_{10}^{\text{CL}}(\tau_1, \tau_2) = -\frac{i}{\hbar} \langle T_c e^{-\frac{i}{\hbar} \int_c H_i(\tau') d\tau'} c_1(\tau_1) a_0^\dagger(\tau_2) \rangle_0$, where the angled brackets $\langle \rangle_0$ indicate ensemble averages with respect to the steady state and the Hamiltonian is separated into $H = H_0 + H_t$, where H_0 is the stationary part and H_t is the time-dependent part. In the nanojunction attached to heat baths, for example, we have $H_t = H_{ep}^C(t)$ while in the nanojunction with an incident photon beam $H_t = H_{ey}^C(t)$.

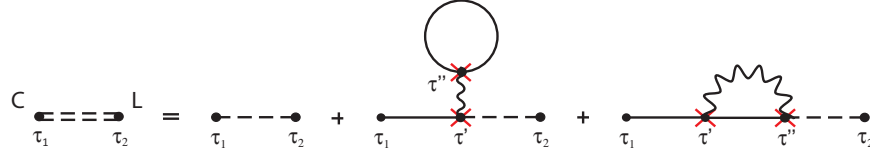


FIGURE 2. Connected diagrams for the perturbation expansion of $G_{10}^{\text{CL}}(\tau_1, \tau_2)$, up to the second-order terms. The wavy lines are the phonon steady-state Green's function and each 3-vertex represents an electron-phonon interaction coupling.

Consider the nanojunction that is attached to heat baths. The perturbation expansion of the contour-ordered Green's function $G_{10}^{\text{CL}}(\tau_1, \tau_2)$ using $H_{ep}^C(t)$ as the perturbing Hamiltonian results in the diagrammatic expansion shown in Fig. 2, up to the second-order term. The expansion translates to

$$G_{10}^{\text{CL}}(\tau_1, \tau_2) = G_{10,0}^{\text{CL}}(\tau_1, \tau_2) - \int_c d\tau' \int_c d\tau'' G_{11,0}^{\text{CC}}(\tau_1, \tau') M_{ep}(\tau') D_{11,0}^{\text{CC}}(\tau', \tau'') G_{11,0}^{\text{CC}}(\tau'', \tau'') M_{ep}(\tau'') G_{10,0}^{\text{CL}}(\tau', \tau_2) + \int_c d\tau' \int_c d\tau'' G_{11,0}^{\text{CC}}(\tau_1, \tau') M_{ep}(\tau') D_{11,0}^{\text{CC}}(\tau', \tau'') G_{11,0}^{\text{CC}}(\tau', \tau'') M_{ep}(\tau'') G_{10,0}^{\text{CL}}(\tau'', \tau_2), \quad (3)$$

where the extra 0 subscript indicates a steady-state Green's function and the phonon steady-state Green's function in the channel $D_{11,0}^{\text{CC}}(\tau_1, \tau_2) = -\frac{i}{\hbar} \langle T_c p_1(\tau_1) p_1^\dagger(\tau_2) \rangle_0$. The diagram containing the fermionic loop vanishes upon integration along the Keldysh contour. We then perform analytic continuation and use Langreth's theorem[1, 2] to Eq. (3) to determine the associated nonequilibrium Green's functions in real time. The lesser nonequilibrium Green's function becomes

$$G_{10}^{\text{CL},<}(t_1, t_2) = G_{10,0}^{\text{CL},<}(t_1, t_2) + \int_0^t dt' \int_0^t dt'' G_{11,0}^{\text{CC},r}(t_1, t') M_{ep}(t') F_{ep}^r(t', t'') M_{ep}(t'') G_{10,0}^{\text{CL},<}(t'', t_2) + \int_0^t dt' \int_0^t dt'' G_{11,0}^{\text{CC},r}(t_1, t') M_{ep}(t') F_{ep}^<(t', t'') M_{ep}(t'') G_{10,0}^{\text{CL},a}(t'', t_2) + \int_0^t dt' \int_0^t dt'' G_{11,0}^{\text{CC},<}(t_1, t') M_{ep}(t') F_{ep}^a(t', t'') M_{ep}(t'') G_{10,0}^{\text{CL},a}(t'', t_2), \quad (4)$$

where

$$F_{ep}^r(t', t'') = D_{11,0}^{\text{CC},<}(t', t'') G_{11,0}^{\text{CC},r}(t', t'') + D_{11,0}^{\text{CC},r}(t', t'') G_{11,0}^{\text{CC},<}(t', t'') + D_{11,0}^{\text{CC},r}(t', t'') G_{11,0}^{\text{CC},r}(t', t''), \\ F_{ep}^<(t', t'') = D_{11,0}^{\text{CC},<}(t', t'') G_{11,0}^{\text{CC},<}(t', t''), \\ F_{ep}^a(t', t'') = [F_{ep}^r(t', t'')]^*. \quad (5)$$

For the nanojunction with an incident photon beam, we can perform a perturbation expansion of $G_{10}^{\text{CL}}(\tau_1, \tau_2)$ with $H_{ey}^C(t)$ as the perturbing Hamiltonian. The diagrammatic expansion results in the same diagrams shown in Fig. 2, up to the second-order terms, except for the reinterpretation of all wavy lines as photon steady-state Green's functions.

There are, however, two versions of each diagram because of the $e^{-i\omega t}$ and $e^{i\omega t}$ coefficients in the electron-photon interaction terms. One diagram is for a forward-moving photon while the other is for a backward-moving photon. Diagrams with fermionic loops do not contribute to the expansion. For this nanojunction, the lesser nonequilibrium Green's function is

$$\begin{aligned} G_{10}^{\text{CL},<}(t_1, t_2) &= G_{10,0}^{\text{CL},<}(t_1, t_2) + \int_0^t dt' \int_0^t dt'' G_{11,0}^{\text{CC},r}(t_1, t') M_{e\gamma}(t') [F_1^r(t', t'') + F_2^r(t', t'')] M_{e\gamma}(t'') G_{10,0}^{\text{CL},<}(t'', t_2) \\ &+ \int_0^t dt' \int_0^t dt'' G_{11,0}^{\text{CC},r}(t_1, t') M_{e\gamma}(t') [F_1^<(t', t'') + F_2^<(t', t'')] M_{e\gamma}(t'') G_{10,0}^{\text{CL},a}(t'', t_2) \\ &+ \int_0^t dt' \int_0^t dt'' G_{11,0}^{\text{CC},<}(t_1, t') M_{e\gamma}(t') [F_1^a(t', t'') + F_2^a(t', t'')] M_{e\gamma}(t'') G_{10,0}^{\text{CL},a}(t'', t_2), \end{aligned} \quad (6)$$

where

$$F_1^r(t', t'') = G_{11,0}^{\text{CC},r}(t', t'') \tilde{D}_{11,0}^{\text{CC},<}(t', t'') + G_{11,0}^{\text{CC},<}(t', t'') \tilde{D}_{11,0}^{\text{CC},r}(t', t'') + G_{11,0}^{\text{CC},r}(t', t'') \tilde{D}_{11,0}^{\text{CC},r}(t', t''), \quad (7)$$

$$F_2^r(t', t'') = G_{11,0}^{\text{CC},<}(t', t'') \tilde{D}_{11,0}^{\text{CC},a}(t'', t') + G_{11,0}^{\text{CC},r}(t', t'') \tilde{D}_{11,0}^{\text{CC},<}(t'', t'), \quad (8)$$

$F_1^a(t', t'') = [F_1^r(t', t'')]^\dagger$, $F_2^a(t', t'') = [F_2^r(t', t'')]^\dagger$, $F_1^<(t', t'') = G_{11,0}^{\text{CC},<}(t', t'') \tilde{D}_{11,0}^{\text{CC},<}(t', t'')$, and $F_2^<(t', t'') = G_{11,0}^{\text{CC},<}(t', t'') \tilde{D}_{11,0}^{\text{CC},>}(t'', t')$, where $\tilde{D}_{11,0}^{\text{CC},>}(t', t'') = [\tilde{D}_{11,0}^{\text{CC},<}(t', t'')]^*$, the modified photon steady-state Green's function $\tilde{D}_{11,0}^{\text{CC},\alpha}(t', t'') = e^{-i\omega t'} D_{11,0}^{\text{CC},\alpha}(t', t'') e^{i\omega t''}$ and $D_{11,0}^{\text{CC},\alpha}(t', t'')$ is the steady-state photon Green's function with $\alpha = r, a, <, >$.

The electron steady-state Green's functions can be built from the adiabatic switch-on of the coupling between the leads and the channel. Since time-translation invariance is satisfied in the steady-state regime, the Fourier transforms of the steady-state Green's functions are well-defined. For the electron CL steady-state Green's functions we get, in Fourier space,

$$\begin{aligned} G_{10,0}^{\text{CL},<}(E) &= G_{11,0}^{\text{CC},r}(E) v_{10}^{\text{CL}} g_{00}^{\text{L},<}(E) + G_{11,0}^{\text{CC},<}(E) v_{10}^{\text{CL}} g_{00}^{\text{L},a}(E), \\ G_{10,0}^{\text{CL},r}(E) &= G_{11,0}^{\text{CC},r}(E) v_{10}^{\text{CL}} g_{00}^{\text{L},r}(E), \\ G_{10,0}^{\text{CL},a}(E) &= [G_{10,0}^{\text{CL},r}(E)]^*, \end{aligned} \quad (9)$$

where the $g_{00}^{\text{L},\alpha}(E)$, $\alpha = r, a, <$, are the equilibrium Green's functions in the left lead. Furthermore, the electron CC steady-state Green's functions are

$$\begin{aligned} G_{11,0}^{\text{CC},<}(E) &= G_{11,0}^{\text{CC},r}(E) \Sigma_{e,11}^{\text{C},<}(E) G_{11,0}^{\text{CC},a}(E), \\ G_{11,0}^{\text{CC},r}(E) &= [(E + i\eta) - \varepsilon_1^{\text{C}} - \Sigma_{e,11}^{\text{C},r}(E)]^{-1}, \\ G_{11,0}^{\text{CC},a}(E) &= [G_{11,0}^{\text{CC},r}(E)]^*, \end{aligned} \quad (10)$$

where the electron self-energy $\Sigma_{e,11}^{\text{C},\alpha}(E) = v_{10}^{\text{CL}} g_{00}^{\text{L},\alpha}(E) v_{01}^{\text{LC}} + v_{12}^{\text{CR}} g_{22}^{\text{R},\alpha}(E) v_{21}^{\text{RC}}$ and the $g_{22}^{\text{R},\alpha}(E)$ are the equilibrium Green's functions in the right lead. The phonon steady-state Green's functions have the same form as the electron steady-state Green's functions except for the substitution of $E \rightarrow \hbar\omega$, $\varepsilon_1^{\text{C}} \rightarrow \hbar k_1^{\text{C}}$, $v_{10}^{\text{CL}} \rightarrow \hbar k_{10}^{\text{CL}}$, $v_{12}^{\text{CR}} \rightarrow \hbar k_{12}^{\text{CR}}$, and the electron self-energy $\Sigma_{e,11}^{\text{C},\alpha}(E)$ to the phonon self-energy $\Sigma_{p,11}^{\text{C},\alpha}(E) = \hbar k_{10}^{\text{CL}} d_{00}^{\text{L},\alpha}(E) \hbar k_{01}^{\text{LC}} + \hbar k_{12}^{\text{CR}} d_{22}^{\text{R},\alpha}(E) \hbar k_{21}^{\text{RC}}$, where the $d_{00}^{\text{L},\alpha}(E)$ and $d_{22}^{\text{R},\alpha}(E)$ are the phonon equilibrium Green's functions in the left and right heat baths, respectively. The photon steady-state Green's functions are also of the same form as the electron steady-state Green's functions except for the substitution of $\varepsilon_1^{\text{C}} \rightarrow \chi_1^{\text{C}}$, $v_{10}^{\text{CL}} \rightarrow u_{10}^{\text{CL}}$, $v_{12}^{\text{CR}} \rightarrow u_{12}^{\text{CR}}$, and the electron self-energy $\Sigma_{e,11}^{\text{C},\alpha}(E)$ to the photon self-energy $\Sigma_{\gamma,11}^{\text{C},\alpha}(E) = u_{10}^{\text{CL}} p_{00}^{\text{L},\alpha}(E) u_{01}^{\text{LC}} + u_{12}^{\text{CR}} p_{22}^{\text{R},\alpha}(E) u_{21}^{\text{RC}}$, where the $p_{00}^{\text{L},\alpha}(E)$ and $p_{22}^{\text{R},\alpha}(E)$ are the photon equilibrium Green's functions in the left and right photon beams.

The electron equilibrium Green's functions can be determined from the equation of motion of the electrons in the leads.[1, 2] For the left lead, we get

$$g_{00}^{\text{L},r}(E) = 2 \frac{(E + i\eta) - \varepsilon_0^{\text{L}}}{v^2} \pm 2i \frac{\sqrt{v^2 - (\varepsilon_0^{\text{L}} - E)^2}}{v^2},$$

$$\begin{aligned}
g_{00}^{L,a}(E) &= [g_{00}^{L,r}(E)]^*, \\
g_{00}^{L,<}(E) &= -f^L(E)(g_{00}^{L,r}(E) - g_{00}^{L,a}(E)),
\end{aligned}
\tag{11}$$

where $f^L(E) = [e^{(E-\mu_L)/k_B T_e^L} + 1]^{-1}$ is the Fermi-Dirac distribution function of the left lead. The equilibrium Green's functions for the right lead are of the same form as those for the left lead except for the replacement of all left-lead parameters into right-lead parameters. The phonon equilibrium Green's functions are of the same form as the electron equilibrium Green's functions except for the substitution of all electron parameters into phonon parameters, the use of the Bose-Einstein distribution function, and taking into consideration that phonon operators follow the commutation rule for bosons. The photon equilibrium Green's functions are of the same form as the phonon equilibrium Green's functions except for the substitution of all phonon parameters to photon parameters.

NUMERICAL RESULTS

To calculate the time-dependent left and right currents we need to determine the lesser nonequilibrium Green's functions $G_{10}^{CL,<}(t_1, t_2)$ and $G_{12}^{CR,<}(t_1, t_2)$. These nonequilibrium Green's functions are expressed as integrals of steady-state Green's functions, as shown in Eqs. (5) and (7). We calculate these integrals numerically using standard integration techniques.[14]

In our calculations, the electron parameters we use are $\varepsilon^L = \varepsilon^R = \varepsilon^C = 0$ and $v^L = v^R = v^C = v^{LC} = v^{RC} = 2$ eV. The left lead parameters are $\mu_L = E_f$ and $T_e^L = 300$ K while the right lead parameters are $\mu_R = E_f - V_b$ and $T_e^R = 300$ K, where the Fermi energy $E_f = 0$ and V_b is the source-drain bias potential.

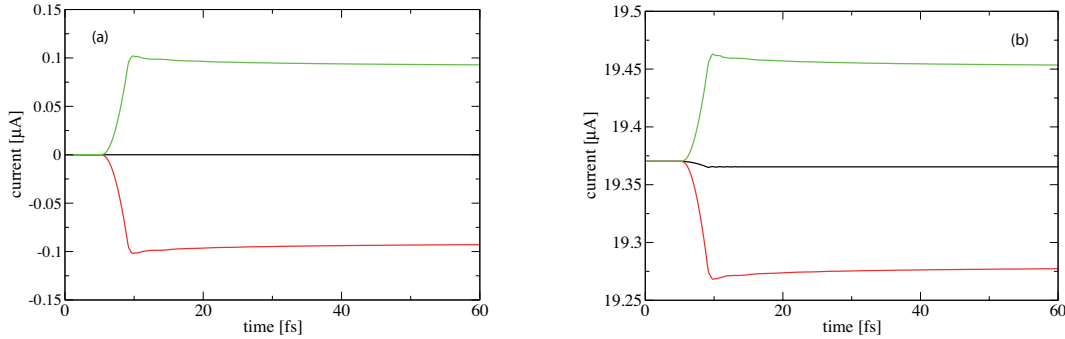


FIGURE 3. The left current (dark line, red online), right current (light line, green online), and average current (black line) for the nanojunction with electron-phonon interactions in the channel is switched on abruptly at 4 fs. The source-drain bias potential in (a) is $V_b = 0$ while in (b) it is $V_b = 0.5$ eV.

Shown in Fig. 3 are the left and right currents in the nanojunction that is attached to heat baths. The phonon parameters we use are $\hbar k^L = \hbar k^R = \hbar k^C = 0.2$ eV and $\hbar \kappa^L = \hbar \kappa^R = \hbar \kappa^C = \hbar \kappa^{LC} = \hbar \kappa^{RC} = 0.5$ eV. The left and right heat bath temperatures are $T_{HB}^L = 473$ K and $T_{HB}^R = 273$ K and the electron-phonon coupling strength is $M_{ep} = 0.5$ eV. Electron-phonon interactions are switched on abruptly, i.e., in the form of a Heaviside step function, at time $t = 4$ fs. Because $T_{HB}^L > T_{HB}^R$, phonons flow from the left heat bath to the right bath. At the channel, the interactions between the electrons and phonons affect the electron current across the device. Shown in Fig. 3(a) are the left and right currents when there is no source-drain bias potential. Since $V_b = 0$, there initially is no current flowing. Then when the electron-phonon interaction is suddenly switched on, electrons start to flow in such a way that the left current is directed towards the left lead and the right current is directed towards the right lead, i.e., the direction of current flow is outwards from the channel, in both directions. The average current $I_{ave} = \frac{1}{2}(I^L(t) + I^R(t))$ remains zero since the form and sign of the left current are exactly the opposite of the right current. Notice also that the currents do not instantly flow when the electron-phonon interaction is abruptly switched on but instead they take time to react, overshoots, and then settle down to steady values. When the nanojunction is attached to a source-drain

bias potential $V_b = 0.5$ eV, we get the currents shown in Fig. 3(b). The left and right currents appear to have the same form. However, the decrease in the left current is more than the increase in the right current thereby resulting in an average current that is less than its original value. The electron-phonon interaction, therefore, gives rise to a resistance that reduces the net current flowing across the device.

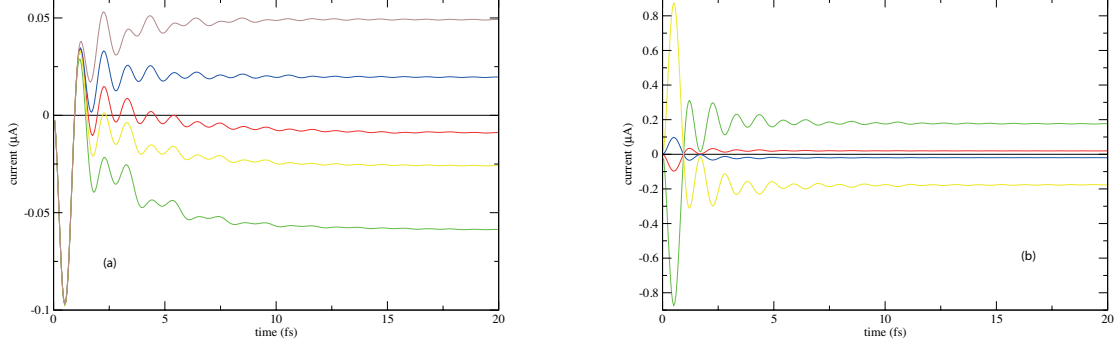


FIGURE 4. (a) The left current in the nanojunction where the photon beam is switched on abruptly at 0 fs. The photon frequencies are 400 THz (red line), 450 THz (green line), 500 THz (blue line), 550 THz (yellow line), and 600 THz (brown line). The Electron-photon coupling is $M_{ey} = 0.5$ eV. In (b), the left (red line) and right (blue line) currents when $M_{ey} = 0.1$ eV and the left (green line) and right (yellow line) currents when $M_{ey} = 0.3$ eV. The photon frequency is 500 THz and $V_b = 0$.

In the nanojunction with an incident photon beam, the photon parameters we use are $\chi^L = \chi^R = \chi^C = 0$ and $u^L = u^R = u^C = u^{LC} = u^{RC} = 0.2$ eV. The electron-photon coupling strength values we investigated are $M_{ey} = 0.1$ eV, 0.3 eV, and 0.5 eV. Shown in Fig. 4(a) are the left current values when the frequencies of the incident photons are varied while the electron-photon coupling is at $M_{ey} = 0.5$ eV. There is no source-drain bias potential. The electron-photon is switched on in the form of a Heaviside step function at time $t = 0$. Notice that when the interaction is switched on the left current dips to a negative value, rises up, oscillates, and then eventually settles down to a steady value. Also notice that the value and direction of flow of the steady-state current depends on the frequency of the incident photons. Shown in Fig. 4(b) are the left and right currents when $M_{ey} = 0.1$ eV and 0.3 eV. Notice that the left current is exactly the opposite of the right current. This means that the left and right currents would both flow into the channel at the same time or both flow out of the channel at the same time, maintaining a zero net current within the channel.

SUMMARY AND CONCLUSION

We are able to calculate the time-dependent current for nanojunctions with dynamical electron-phonon and electron-photon interactions. We use the two-time nonequilibrium Green's functions to calculate the current. We find that the current takes time to react to a sudden change in the device. The current would overshoot, oscillate, and then settle down to a steady value. Electron-phonon interactions drive the electrons out of the channel and result in a net resistance to the current flow whenever a source-drain bias potential is present. Electron-photon interactions also pushes the electron current to flow. The direction of flow, however, depends on the frequency of the incident photons. Furthermore, the direction of current flow in one lead is opposite to the direction of current flow in the other lead, thereby resulting in no net current within the channel.

ACKNOWLEDGMENTS

CML would like to acknowledge support from the Accelerated Science and Technology Human Resources Development Program of DOST-SEI.

REFERENCES

- [1] H. Haug and A.-P. Jauho, *Quantum Kinetics in Transport and Optics of Semiconductors* (Springer, Berlin, 2008).
- [2] G. Stefanucci and R. van Leeuwen, *Nonequilibrium Many-Body Theory of Quantum Systems: A Modern Introduction* (Cambridge University Press, U.K., 2013).
- [3] A.-P. Jauho, N.S. Wingreen, and Y. Meir, *Phys. Rev. B* **50**, 5528–5547 (1994).
- [4] J. Maciejko, J. Wang, and H. Guo, *Phys. Rev. B* **74**, 085324 (2006).
- [5] A. Crépieux, Šimkovic, B. Cambon, and F. Michellini, *Phys. Rev. B* **83**, 153417 (2011).
- [6] E.C. Cuansing and G. Liang, *J. Appl. Phys.* **110**, 083704 (2011).
- [7] D. Kienle, M. Vaidyanathan, and F. Léonard, *Phys. Rev. B* **81**, 115455 (2010).
- [8] L.E. Henrickson, *J. Appl. Phys.* **91**, 6273–6281 (2002).
- [9] E.C. Cuansing, *Int. J. Mod. Phys. B* **31**, 1750105 (2017).
- [10] J.M. Ziman, *Principles of the Theory of Solids*, 2nd ed. (Cambridge University Press, Cambridge, U.K., 1972).
- [11] O. Madelung, *Introduction to Solid State Theory* (Springer, Berlin, 1978).
- [12] J.T. Lü and J.-S. Wang, *Phys. Rev. B* **76**, 165418 (2007).
- [13] M. Galperin and A. Nitzan, *Phys. Chem. Chem. Phys.* **14**, 9421–9438 (2012).
- [14] W.H. Press, S.A. Teukolsky, W.T. Vetterling, and B.P. Flannery, *Numerical Recipes: The Art of Scientific Computing*, 3rd ed. (Cambridge University Press, Cambridge, U.K., 2007).